Numerical 3D simulation of the NPSH characteristics of centrifugal pumps with local and integral analysis of void structures

[1]Phillip Limbach*; [1]Romuald Skoda;

[2]Tim F. Groß; [2]Gerhard Ludwig; [2]Peter F. Pelz

[1]*Chair of Hydraulic Fluid Machinery, Ruhr-Universität Bochum, Universitätsstr. 150, 44801 Bochum, Germany;*

[2]*Chair of Fluid Systems, Technische Universität Darmstadt, Otto-Berndt Str. 2, 64287 Darmstadt, Germany*

Abstract

3D numerical simulations with mass transfer cavitation model are performed in a centrifugal pump (n_q=26 min^{-1}). Simulation results are compared to measurements of *NPSH* characteristics and optical measurements of void structures. Transient single bubble cavitation is observed in the experiments with hydraulically smooth blades, whereas in the simulations, the cavitation region appears as stationary sheet cavitation for the entire operation range. Local cavitation structures in the impeller are spatially integrated for measurements and simulation results. The resulting cavitation intensity provides additional information on the extent of cavitation zones at *NPSH* levels well above $NPSH_{3\%}$, where the head is yet unaffected by cavitation. The $NPSH_{3\%}$ curve as well as cavitation intensity are well predicted, although local void structures show a mismatch to measurements.

Keywords: centrifugal pump, mass transfer cavitation model, NPSH, void structures, cavitation intensity

1. Introduction

Different cavitation regimes may develop in centrifugal pumps varying in their transient occurrence and erosive impact. An accurate prediction of the cavitation dynamics is therefore of particular importance for reliable pump design and performance. For the prediction of cavitation in centrifugal pumps, URANS methods in combination with mass transfer models that are based on simplified bubble dynamics, i.e. Rayleigh equation [1], are the most commonly used model class, because of the moderate computational effort. Due to crucial simplifications in this approach, modifications of the cavitation model parameters and mixture eddy viscosity may be necessary to capture the relevant flow characteristics, e.g. cloud cavitation [2–4]. Cavitation model parameter variations for centrifugal pump flow usually aim at matching the measured $NPSH_{3\%}$ [5, 6] and do not consider local cavitation structures. Therefore, in the present study, an evaluation of void structures is performed in addition to *NPSH* characteristics.

As found in previous investigations of the present authors [7] the reduction of the mixture eddy viscosity [2, 3] is indispensable for the prediction of cloud cavitation at external (i.e. hydrofoil) as well as internal flow (i.e. orifice flow). In order to capture cloud cavitation over a wide range of operation points and at the same time accurately predict the mass flow rate, a modification of the pre-factors for evaporation and condensation in the cavitation model is necessary, leading to different parameter sets for hydrofoil and orifice flow. However, the mass flow rate prediction is predominantly influenced by the turbulent wall treatment, rather than by the cavitation model modifications, i.e. a low-Re approach is indispensable if viscous flow separation is present. The mass flow rate at choking conditions in the orifice is well predicted even with original cavitation model parameters and un-modified mixture eddy viscosity. Transferring these findings to cavitating low specific speed pump flow with n_q=12 min^{-1} [8], we confirmed that a low-Re approach is in fact indispensable for an accurate prediction of choking and $NPSH_{3\%}$ at overload operation, because cavitation zones switch from the impeller to the volute tongue, where significant incidence and viscous separation occur. On the other hand, wall functions are appropriate for moderate incidence flow in the impeller as far as no viscous separation occurs.

To evaluate these conclusions of the previous studies, in the present study a centrifugal pump with n_q=26 min^{-1} is investigated, where no significant viscous flow separation is present at the considered operation points. Local

*Corresponding Author, Phillip Limbach: phillip.limbach@rub.de

visualizations of the cavitation zones are used to validate and assess the simulation results concerning the head drop mechanisms.

2. Experimental setup

The centrifugal pump with specific speed of n_q=26 min^{-1} is part of the closed-loop test rig at the chair of Fluid Systems of the Technical University of Darmstadt. A wide range of rotational speeds, flow rates and gap sizes between the impeller shroud and casing at the suction side have been considered. A detailed description of the test rig, experimental setups as well as a comprehensive discussion of the results is provided by e.g. [9] and briefly summarized in the following. The pump is equipped with a six blade impeller. The impeller outlet diameter and outlet width are D_2=260 mm and b_2=23.5 mm, respectively. A sketch of the pump and an image of the impeller with de-mounted shroud is presented in Fig. 1a. A rotation-symmetrical annulus chamber instead of a volute yields essentially uniform flow conditions in circumferential direction downstream of the impeller. The casing is connected to the pressure pipe via twelve outflow tubes, which are distributed symmetrically over the casing. The static outlet pressure p_{out} is measured at D_{out}=500 mm in the annulus chamber and the static pressure on the suction side p_s is measured in the suction pipe ~550 mm upstream of the impeller inlet. The nominal load operation points at rotational speeds of n=1750 min^{-1} and n=2000 min^{-1} are specified as Q_{opt}=125 m³/h and Q_{opt}=143 m³/h, respectively. A transparent suction pipe, front casing and shroud are utilized, and cavitation voids are visualized using stroboscopic lighting and a 90° borescope that is positioned in front of the impeller. A high-speed camera system enables image recordings with 10,600 frames per second and a resolution of 1920x1080 pixels. The experiments in the present study are primarily performed with hydraulically smooth blades. The impeller suction side roughness has been varied exemplarily by applying thin layers of glue and small particles of silicon carbide with a particle size of 125 μm that are distributed over a distance of 3 mm from the leading edge.
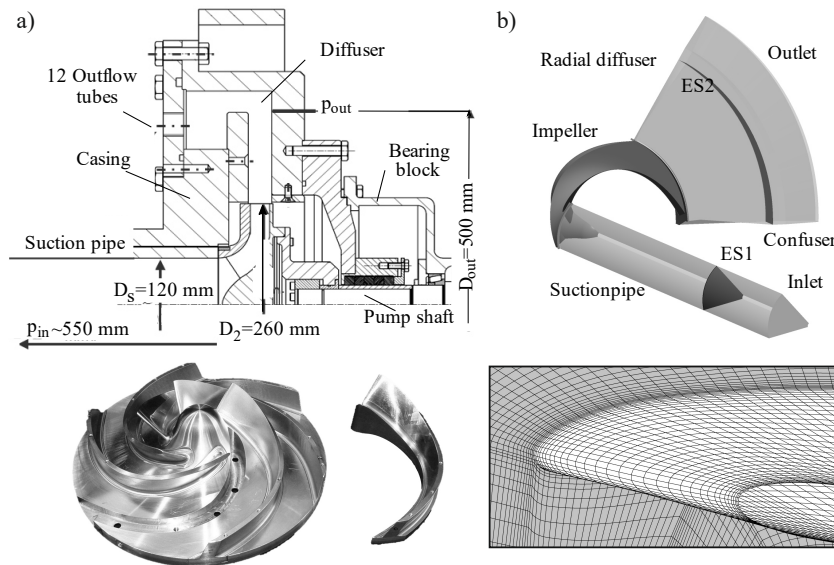

Fig. 1: a) Section view of the centrifugal pump and image of the impeller with de-mounted shroud; b) Computational domain and grid details of grid G02 in the vicinity of the leading edge.

3. Numerical setup

Due to the rotation-symmetrical annulus chamber, periodic flow conditions are assumed and only one impeller channel (60° segment) is considered in the numerical model applying periodic boundary conditions in circumferential direction, see Fig. 1b. The suction pipe and the discharge of the impeller channel are elongated to reduce the influence of the boundary conditions on the impeller flow. A confuser is added at the radial outlet section to avoid positive pressure gradients in that region. A block structured grid with a resolution of approximately 55,000 (G01) and 480,000

*Corresponding Author, Phillip Limbach: phillip.limbach@rub.de

(G02) nodes is used, see Fig. 1b. The grid G02 is generated by halving the length of the cell edges of grid G01 in all directions. No significant grid dependence could be observed for the subsequently discussed results, so that only G02 results are presented in section 4. According to the experiments, different gap sizes, s, are considered in the numerical model (s=0; 0.15; 0.2 mm). Simulations are performed with the commercial flow solver ANSYS CFX 16.1 and cavitation model of [10]. Since previous studies [7, 8] revealed that choking mass flow rate is well predicted by default settings, the default pre-factors for evaporation (F_{vap}=50) and condensation (F_{cond}=0.01) are maintained, and no modification of the mixture eddy-viscosity is done. Normal velocity is specified at the inlet and static pressure is defined at the outlet, which is successively reduced in several simulation runs for the calculation of the head drop and $NPSH_{3\%}$. The k-ω SST turbulence model is applied with an automatic wall treatment [11, 12]. Although all simulations are performed in the relative frame of reference, transient simulation runs are performed because for several stationary simulations, the residuums do not drop by more than two orders of magnitude. Second order schemes are used for spatial and temporal discretization. The convergence criterion is set to a drop of maximum residuum R_{Max} by four orders of magnitude and imbalances < 1%. The head H, is evaluated in accordance to the experiments by the static pressure difference between pressure and suction side $p_{s,ES1,2}$. The $NPSH$ is determined by the difference between total pressure on the suction side, $p_{t,ES1}$, and the vapor pressure, p_v.

4.   Results

For experiments with hydraulically smooth surface, single bubble cavitation is primarily observed, see Fig. 2a and for details [9], and no cloud cavitation is observed. These bubbles appear to be inherently unsteady, even after transformation of the images into the relative frame of reference, i.e. rotating every picture against the direction of rotation to a certain amount to freeze the impeller.
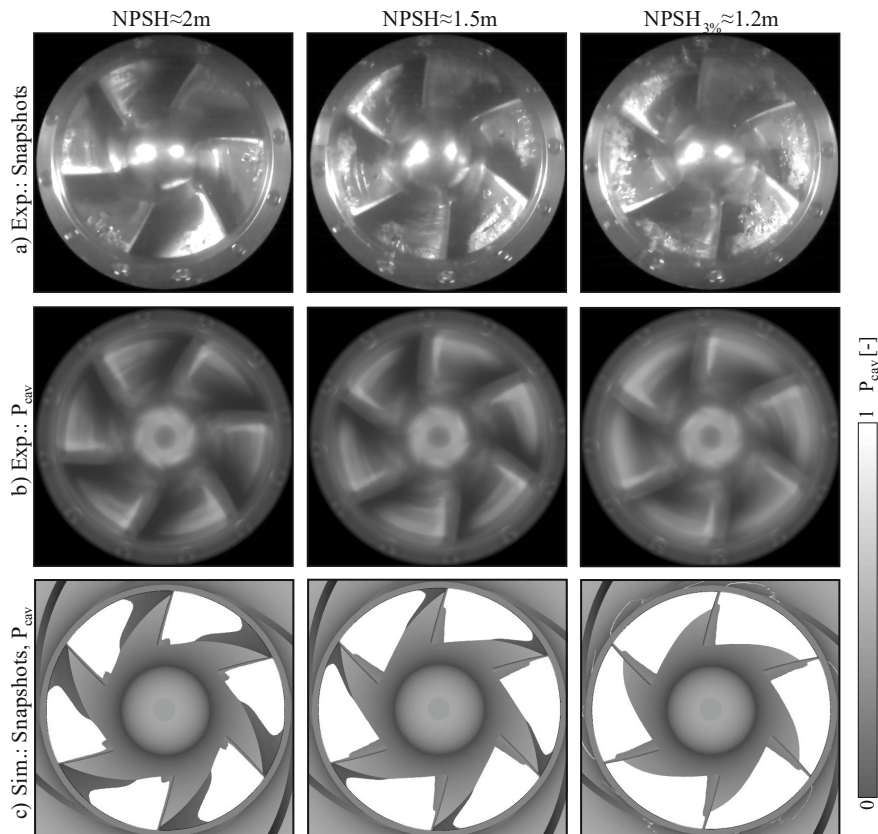

Fig. 2: a) Snapshots of the cavitating flow at arbitrary time instances and b,c) cavitation probability, P_{cav}, for varying NPSH. The single-channel simulation results are copied in circumferential direction according to the number of blades for a full-impeller illustration and comparison with measurements.

*Corresponding Author, Phillip Limbach: phillip.limbach@rub.de

The simulations a priori cannot capture this cavitation regime with distinct single bubbles, due to the assumption of a homogenous mixture, e.g. a particular amount of individual bubbles and nuclei within each computational cell [10]. Hence, the simulation results show essentially stationary cavitation sheets, which are attached at the blades and illustrated in Fig. 2c by means of iso-surfaces of 10% void volume fraction. Note that the absence of transient cavitation patterns in the impeller simulation is not necessarily only a consequence of model simplifications, since results of preliminary simulations with cavitation model settings adopted from [7, 8], i.e. parameters optimized for cloud cavitation simulations and a locally reduced mixture eddy-viscosity, show essentially stationary cavitation sheets as well.

The $NPSH_{3\%}$ is predicted accurately over a wide range of normalized operation points $q = Q/Q_{opt}$ and gap widths, as shown in Fig. 3 and discussed in the following. The influence of the grid resolution on $NPSH_{3\%}$ is below $\Delta NPSH_{3\%} < 1\%$ and therefore minor (not shown). Although the cavitation regime is predicted to be stationary in contrast to the measurements, the time-averaged spatial extent of the measured cavitation zones, represented by the cavitation probability, P_{cav}, is qualitatively well predicted, see Fig. 2b and c. The cavitation probability is evaluated equally in measurement and simulation: by averaging the grayscale of a pixel over a distinct number of single-shot images, it provides the qualitative distribution of the probability of the existence of voids at a certain location. Due to essentially stationary voids in the simulation results, P_{cav} in Fig. 2c is essentially identical to the instantaneous images of void fraction iso-surfaces. Note that the background grayscale is not subtracted from the cavitation probability and the impeller also appears gray in Fig. 2b and c. At ~$NPSH_{3\%}$, the cavitation structures on the suction side extend to the impeller throat area, leading to choking and the head drop. The decrease of $NPSH_{3\%}$ due to closing the gap is captured qualitatively by the simulations. Interestingly, the application of modified cavitation model parameter sets for the prediction of cloud cavitation [7, 8] does not lead to significant differences of both, $NPSH_{3\%}$ and the local cavitation structures.
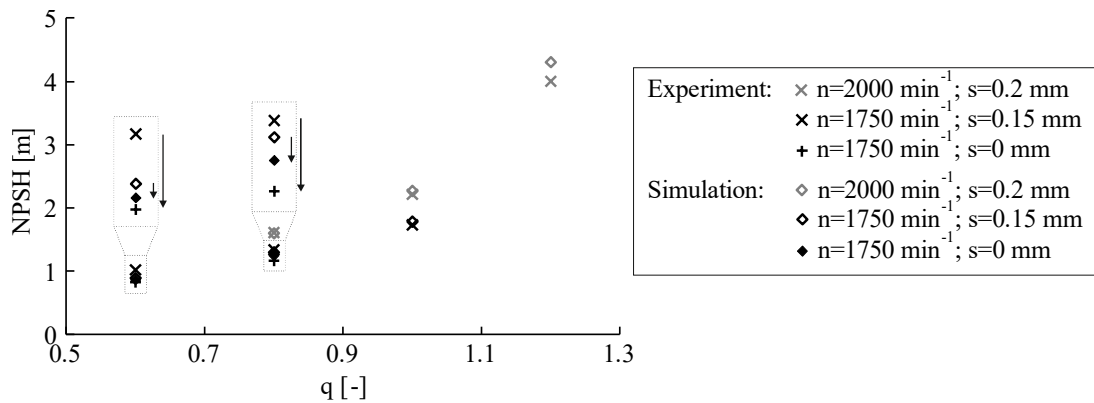

Fig. 3: $NPSH_{3\%}$ curve for different rotational speeds (n=1750; 2000 min^{-1}) and gap widths (s = 0, 0.15 and 0.2 mm)

For a quantitative analysis at q=0.6 and 0.8, Fig. 4 shows the cavitation intensity, I_{cav}, that is evaluated by integrating the grayscale values over all pixels of P_{cav} in the experiments. In the simulations, the vapor volume fraction is integrated over the computational domain and subsequently time-averaged to evaluate I_{cav}. For a comparison of simulation and measurement results, I_{cav} is normalized. For experimental data, the background intensity, I_{ref}, i.e. the cavitation intensity at a high pressure level and single-phase flow conditions, is substracted from the respective I_{cav} values before normalization. Normalization to I_{cav} e.g. at 3% head drop ($NPSH_{3\%}$) is not appropriate, because cavitation zones on the pressure side of the blades as well as in the impeller throat area are not visible in the experiments and therefore do not contribute to the evaluation of I_{cav}. On the other hand, these hidden voids do contribute to the evaluation of I_{cav} in the simulations. For $NPSH$=1.5 m, the cavitation zones do not extend to the throat area of the impeller. According to the simulation results, no cavitation is observed on the pressure side of the impeller blades. Therefore, I_{cav} is normalized by $I_{cav,1.5}$ at $NPSH$=1.5 m, where no head drop is discernible yet.

*Corresponding Author, Phillip Limbach: phillip.limbach@rub.de

$I_{cav}/I_{cav,1.5}$ thus per definition equals one at $NPSH$=1.5 m, for measurement and simulation. A good agreement between simulations and experiments is obtained for both flow rates, q=0.6 and 0.8, at high and moderate $NPSH$, see Fig. 4. The cavitation intensity is slightly overestimated at low $NPSH$ values. We attribute this overestimation to the limited visual access in the experiments, as described above.

In Fig. 4, the head drop curves are also included and show essentially the same drop of H for measurement and simulations, resulting in good agreement of $NPSH_{3\%}$ in Fig. 3. A significant head drop occurs rather abruptly only at low $NPSH$ levels where pronounced void structures are present. Thus, the cavitation intensity provides additional information on the extent of cavitation at $NPSH$ levels, where smaller cavitation zones are present that do not influence the pump performance yet.
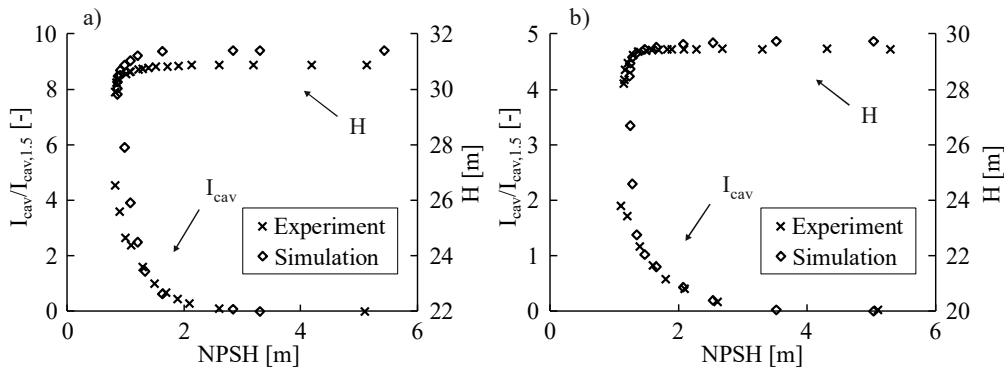

Fig. 4: Cavitation intensity, I_{cav}, for n=1750 min^{-1} and s=0 mm, at a) q=0.6 and b) q=0.8.

Interestingly, the inclusion of roughness elements at the leading edge of the impeller blades leads to the occurrence of sheet cavitation even in the measurements (details are available in [9]) and a good agreement to the cavitation zones that are observed in the simulations, as exemplarily shown in Fig. 5. We attribute this to a more homogeneous distribution of nuclei at the roughness elements and wall crevices along the leading edge and therefore a better fulfilment of one main assumption of the cavitation model, i.e. a homogenous nuclei distribution within each computational cell. A general analysis of the role of surface nuclei for the inception of hydrodynamic cavitation has recently been studied by some of the authors of this paper [13].
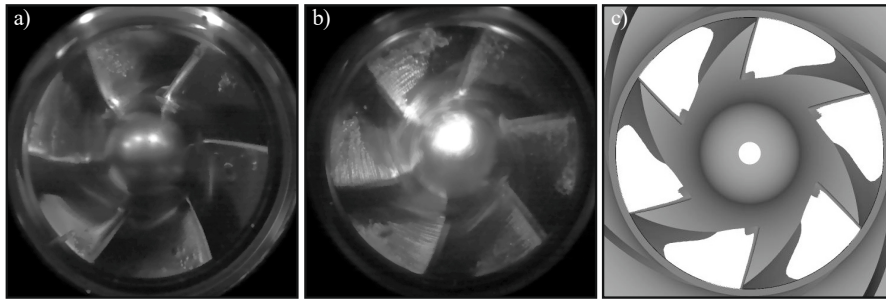

Fig. 5: Exemplary snapshots of the local cavitation structures on the suction side of the impeller blades at n=1750 min^{-1}, q=0.8, s = 0 mm and $NPSH$ =2 m; a) smooth blades; b) roughened leading edge on the suction side; c) simulation results.

5. Conclusion

In addition to head drop and $NPSH_{3\%}$ characteristics, the cavitation probability and intensity provide complementary information on the extent of cavitation zones at moderate $NPSH$ levels, where the head is not yet affected by cavitation. Although the highly unsteady appearance of the cavitation zones for smooth surface is not reflected by the simulation results, the head drop and $NPSH_{3\%}$ characteristics are well predicted. In former investigations this holds even for cloud cavitation [7] where the low-Reynolds resolution of viscous wall boundary layer separation has been shown to

*Corresponding Author, Phillip Limbach: phillip.limbach@rub.de

be more critical for $NPSH_{3\%}$ prediction than the resolution of unsteady shedding of voids. Since for the operation conditions considered in the present study viscous separation is not significant, the utilization of turbulent wall functions seems feasible. It may be concluded that for prediction of $NPSH_{3\%}$ and even for prediction of integral void structures it may be sufficient to capture the time-averaged spatial extent of the cavitation zones, without capturing the unsteady cavitation regime. This assumption need to be verified for a wider operation range and range of specific speeds in further studies.

6. References

[1]   Rayleigh (1917). *On the pressure developed in a liquid during the collapse of a spherical cavity.* Philosophical Magazine Series 6; 34, 94–8.

[2]   Reboud, J. L., Stutz, B., Coutier, O. (1998). *Two-phase flow structure of cavitation: Experiment and modeling of unsteady effects.* In 3rd International Symposium on Cavitation, Grenoble, France.

[3]   Coutier-Delgosha, O., Fortes-Patella, R., Reboud, J. L. (2003). *Evaluation of the Turbulence Model Influence on the Numerical Simulations of Unsteady Cavitation.* Journal of Fluids Engineering; 125, 38–45.

[4]   Frikha, S., Coutier-Delgosha, O., Astolfi, J. A. (2008). *Influence of the Cavitation Model on the Simulation of Cloud Cavitation on 2D Foil Section.* International Journal of Rotating Machinery; 2008, 1–12.

[5]   Chatagny, L., Berten, S. (2016). *Challenges and open questions in cavitation simulations for centrifugal pump applications.* In 3rd International Rotating Equipment Conference (IREC), Pumps, Compressors and Vacuum Technology, 765–75, Düsseldorf, Germany.

[6]   Salvadori, S., Cappelletti, A., Martelli, F., Nicchio, A., Carbonino, L., Piva, A. (2012). *Numerical prediction of cavitation in pumps.* In 15th International Conference on Fluid Flow Technologies, Budapest, Hungary.

[7]   Limbach, P., Skoda, R. (2017). *Numerical simulation of cloud cavitation in hydrofoil and orifice flows with analysis of viscous and non-viscous separation.* Journal of Fluids Engineering; submitted.

[8]   Limbach, P., Skoda, R. (2017). *Numerical and experimental analysis of cavitating flow in a low specific speed centrifugal pump with different surface roughness.* Journal of Fluids Engineering; 139, 101201.

[9]   Groß, T., Ludwig, G., Pelz, P. (2016). *Influence of surface roughness on cavitation in a centrifugal pump.* In 3rd International Rotating Equipment Conference (IREC), Pumps, Compressors and Vacuum Technology, 801–11, Düsseldorf, Germany.

[10] Zwart, P. J., Gerber, A. G., Belamri, T. (2004). *A two-phase flow model for predicting cavitation dynamics.* In 5th International Conference on Multiphase Flow, Yokohama, Japan.

[11] Menter, F. R. (1994). *Two-equation eddy-viscosity turbulence models for engineering applications.* AIAA Journal; 32, 1598–605.

[12] Menter, F. R., Kuntz, M., Langtry, R. (2003). *Ten years of industrial experience with the SST turbulence model.* Turbulence, heat and mass transfer; 4, 625–32.

[13] Groß, T. F., Pelz, P. F. (2017). *Diffusion-driven nucleation from surface nuclei in hydrodynamic cavitation.* Journal of Fluid Mechanics; 830, 138–64.

*Corresponding Author, Phillip Limbach: phillip.limbach@rub.de